Geology
June 2016, Volume 44 Issue 6 Pages 423-426
http://dx.doi.org/10.1130/G37585.1
http://archimer.ifremer.fr/doc/00345/45668/

Tectonic regime controls clustering of deformation bands in porous sandstone

Soliva Roger [1], Ballas Gregory [2], Fossen Haakon [3, 4], Philit Sven [1]

[1] Univ Montpellier, Geosci Montpellier, Campus Triolet,CC060,Pl Eugene Bataillon, F-34095 Montpellier 05, France.
[2] Inst Francais Rech Exploitat Mer, F-29280 Plouzane, France.
[3] Univ Bergen, Dept Earth Sci, Allegaten 41, N-5007 Bergen, Norway.
[4] Univ Bergen, Museum Nat Hist, Allegaten 41, N-5007 Bergen, Norway.

Abstract :

Porous sandstones tend to deform by the formation of low-permeability deformation bands that influence fluid flow in reservoir settings. The bands may be distributed or localized into clusters, and limited recent data suggest that tectonic regime may exert control on their distribution and clustering. In order to explore this suggestion, we performed a synthetic analysis based of 73 sets of bands, including 22 new sets measured for a reverse Andersonian regime that fill the important gap in data for this context. We find a surprisingly strong correlation between clustering and tectonic regime, where bands clearly are more distributed in the reverse regime compared to the normal regime. Together with the observed band distributions, capillary pressure data show evidence that efficient membrane seals are expected for extension, whereas pervasive permeability anisotropy is expected for contraction. Such a basic new rule concerning tectonic regime is very useful for assessment of reservoir properties where deformation bands are common but below seismic resolution.

INTRODUCTION

Tectonic deformation in porous sandstones generally produces cataclastic deformation bands in which grain crushing, sliding and rolling take place (Aydin, 1978; Fossen et al., 2007). The result is typically grain size reduction that causes porosity loss and reduction of permeability by up to 6 orders of magnitude (Fossen and Bale, 2007; Ballas et al., 2015). Different classes of cataclastic deformation bands have been recognized as a function of their relative amount of shear to compaction, including shear bands (SB), compactional shear bands (CSB), shear enhanced compaction bands (SECB) and pure compaction bands (PCB) (Eichhubl et al., 2010; Soliva et al., 2013). Some of their properties, such as their displacement–length scaling relationship (Schultz et al., 2008), degree of cataclasis, petrophysical properties (Ballas et al., 2014) and spatial distribution (Fortin et al., 2005; Saillet and Wibberley, 2010) seem directly linked to such differences in kinematics. Identifying the internal and external factors controlling such differences in band kinematics could then be of first-order importance for sandstone reservoir characterization.

Both mechanical tests and field data in porous sandstones suggest that many factors, including grain size, porosity, proximity to faults, segmentation, burial depth, and potentially also fluid pressure, are thought to influence the spatial distribution of deformation bands and their relative amount of shear to compaction (e.g., Wibberley et al., 2007; Solum et al., 2010; Nicol et al., 2013; Soliva et al., 2013; Ballas et al., 2014). In this paper we inspect the role of tectonic regime on the spatial distribution of deformation bands with new data collected from 22 outcrops in contractional settings in California, Nevada, France, Germany and Taiwan. This allows for a sound synthetic analysis of band distribution in reverse regime compared to data in normal regimes collected from the literature. We briefly discuss the origin of the observed general trend and implications for sandstone reservoirs.

GEOLOGIC SETTINGS

Band frequency data (number of bands per meter) were measured in Nevada in the fine to medium grained porous Jurassic Aztec Sandstone (Fossen et al., 2015). This unit has been involved in the Cretaceous Sevier orogeny, with the east to southeast transport of the Muddy Mountain thrust sheet. Data have been collected from 3 principal sites, one in the Buffington window and the two others in the Valley Of Fire State Park.

In California, data were collected from oil-filled porous sandstones of the Edna Member of the Mio-Pliocene Pismo Basin (Antonellini et al., 1999). This basin occupies a syncline limited by the Edna thrust fault to the northeast. Layers containing deformation bands show a wide range in grain size (fine-grained sand to gravel). Measurements were made on one outcrop but are separated into 3 sets because of the different band distributions observed in the different layers.

In France we measured band sets in the porous Cretaceous sandstones of the South East Basin (Ballas et al., 2014). These marine sandstones have been folded and faulted during the N-S Paleocene-Eocene Pyrenean shortening, and data from 8 outcrops are reported here for host rocks showing medium to coarse grain sizes.

Data from Germany were collected from the Subhercynian Alpine basin in the medium-size porous sandstones of the lower Cretaceous Involutus and Heidelberg formations (Klimczak and Schultz, 2013). This basin is folded and mainly faulted at its Southwestern border by the Harz Mountain thrust. Data reported in this paper are from 4 outcrops observed at different places in the basin, with one outcrop very close to the Harz thrust and 3 others relatively far from the thrust (> 2 km).

Cataclastic bands from Taiwan are located on the East Coast (Shihtiping), in fine- to coarse-grained volcanic-tuff sandstones. These deposits are related to the formation of the Coastal Range due to the arc-continent collision ~7 million years ago. A N-S striking fold affects these deposits and 2 band sets were measured in the site.

BAND SET GEOMETRY, FREQUENCY AND CLUSTERING

Method

Because many workers have counted the number of individual bands per meter, we proceed in the same way, using a tape ruler along outcrops, to allow for a global data synthesis. Most data sets from the Andersonian normal stress regime are acquired along scan lines oriented along the direction of maximum extension (X-axis of the strain ellipsoid). For the new measurements provided for the Andersonian reverse stress regime, we counted the bands along a scan line oriented along the direction of maximum shortening (Z-axis).

Band Set Geometry

Outside of fault zones, cataclastic deformation bands forming reverse band sets are generally pervasive sets of SECBs or CSBs. SECBs generally show no visible displacement in the field and outcrop as conjugate sets that intersect only in some parts of the outcrops (Fig. 1a). CSBs generally outcrop as regular mesh-like geometries of conjugate crosscutting bands (Fig. 1b), along which reverse sense displacement of a few centimeters can be observed. Both types of band sets are very rare in fine sandstones, and are generally restricted to specific layers of medium to coarse porous sandstone. Within the deformed layers, the spatial distribution of the bands is extensive, generally over entire outcrop exposures (tens to a hundred meters) with more or less evenly spaced bands (Figs. 1a and 1b). Note however that SBs organized as clusters can also be observed in reverse regime, but specifically located within fault zones (see Figure 1e Subhercynian).

Bands in the normal regime are typically CSBs and SBs clustered around normal faults, defining damage zones. Damage zones are characterized by a steep increase in band density toward a main fault surface, which is located along or within a central cluster zone (Figs. 1c and 1d). In addition, clusters can also occur as incipient fault structures far from established fault surfaces. SBs in the clusters are spaced a few millimeters or centimeters apart, and generally oriented subparallel to the fault. Bands can form parallel or conjugate sets, branching or as mutually crosscutting structures (Fig. 1b). These SBs can show centimeter- to decimeter-scale displacements and generally display more intense cataclasis than CSBs and SECBs.

Histograms of number of bands per meter are shown in Figure 1e for some of the most representative reverse band sets. These graphs show nearly homogeneous to polymodal distribution with some modes that are located at places where few faults or ladder structures are observed (see Schultz and Balasko, 2003 for definition of ladder structure). For all the reverse band sets reported in the literature (see Figure 2 for references), the mean value of bands per meter is 12, with a standard deviation of 9.6. The spatial distribution is particularly heterogeneous in outcrops showing variations in lithology such as the case of the Pismo Basin (Fig. 1e). Relatively high values of bands per meter are observed in medium-grained units (generally >10 bands/m), while lower band frequencies are observed in coarse-grained units (generally <10 bands/m), and few bands are observed in the sand matrix of gravel units. Fine sandstones, cemented sandstones or other low-porosity rock layers are devoid of SECBs or CSBs.

The distribution of normal sense bands per meter appears Gaussian or Log-Normal like; see Figure 1f for some of the most representative normal band sets measured. These modal distributions generally show a progressive increase in band density to a maximum value (cluster), into which bands are very closely packed (Fig. 1c). An asymmetric distribution (Log-Normal distribution type) generally reflects the juxtaposition of differently damaged units around a fault surface. For all the normal band sets collected from the literature (Fig. 2), the maximum number of bands per meter reaches the value of 161. Also note that zones devoid of bands are frequently reported on the graphs presented in Figure 1f.

Data Synthesis Analysis

We have synthetized all the band density data obtained from our own field work and from the literature, altogether 24, 47 and 2 band sets from the reverse, normal and strike-slip regime, respectively. These 73 sets represent a total of 27074 bands recorded along scan lines from sandstones showing a wide range in porosity (18.6 – 35.14%), grain size (0.24 mm in diameter to gravels), burial depth (0.3 – 2.5 km) and diagenetic context.

To precisely examine the relative spatial distribution of bands of all sets together, we calculate the “cluster factor” (Wibberley et al., 2007) for each set. This parameter is a standard deviation-type function describing the degree of clustering within a given band set along a scan line. The “cluster factor” is defined as:

$$Cf = \sqrt{\left(\frac{\sum f_i^2}{\sum f_i} - f_{av}\right)} \quad . (1)$$

in which f_i is the number of bands encountered per meter of scan line, i represents the i^{th} meter interval along the scan line, and f_{av} is the average band frequency for the entire scan line. For all the band sets collected and measured, this factor varies between 0.47 and 8.78, where 8.78 corresponds to the highest band clustering and 0.47 is the most even band distribution.

A global data analysis shows a clear difference between reverse and normal band sets with respect to spatial distribution. Figure 2 presents all band sets measured by us and collected from the literature as a function of the *cluster factor* and the *maximum value of bands per meter*. This graph reveals that reverse band sets (black dots) have low *cluster factor*, but also low values of *maximum band per meter* as compared to normal band sets. Reverse band sets have cluster factor values between 0.4 and 2.8, with ~25% of the sets having values >2, and a *maximum band per meter* ranging from 6 to 67, with ~70% of the sets having values <30. In contrast, normal band sets have cluster factor values between 1.4 and 8.8, with >80% having values higher than 2, and *maximum band per meter* ranging from 9 to 161, with ~70% having values >30. This synthetic data set analysis shows two different and little-overlapping graphical domains for reverse and normal band sets, revealing that sets formed in the reverse tectonic regime (contraction) are generally more spatially distributed than sets formed in the normal tectonic regime (extension). Large *cluster factor* values seem possible also for the strike-slip regime.

Beyond the fact that the amount of strike-slip data has no significant statistical weight, this low amount of data allows questioning the extent of their occurrence in porous sandstones.

DISCUSSION

The global data set presented in Figure 2, clearly shows that reverse bands are more spatially distributed than normal bands, which are characterized by more clustered distributions. This difference in organization reveals that tectonic regime is a prominent factor for the distribution of deformation bands in porous sandstone. However, the presence of faults and even primary lithologic heterogeneities seem to be factors that can influence the distribution of bands in reverse band sets (Fig. 1e), but do not control the general trend. On the other hand, spatially distributed band sets have also been observed in extensional settings, but in specific settings such as in relay zones (e.g., Davatzes and Aydin, 2003, open dot noted 4 in Fig. 2) or in cases where strong lithological contrasts impede the propagation of SBs (Schultz and Fossen, 2002).

This influence of tectonic context can be explained by the difference in stress paths occurring in sandstone under normal and reverse tectonic regimes (Soliva et al., 2013). Indeed, relatively low mean stress inherent to tectonic extension lead to a localized Byerlee-type cataclastic-shear behavior, whereas high mean stress promoted by tectonic contraction lead to distributed compactional/cataclastic behavior (see supplementary material for the mechanical explanation and Wong and Baud, 2012 for the behavior of porous sandstones). This analysis therefore suggests that remote tectonic stress has a stronger influence on band distribution in general than local stress, such as provided by reactivation of inherited faults, layering or fault segmentation.

Because deformation bands are well known to be subseismic structures, the exposed evidences of different strain localization, together with differences in petrophysical properties between shear-dominated and compaction-dominated bands, provide important conclusions for the management of sandstone reservoirs. Recent data compilation shows that permeability is significantly lower into shear-dominated bands compared to compaction-dominated bands (Ballas et al., 2015), but rather than permeability, capillary pressure is an efficient indicator of the ability of a fault to act as a barrier to fluid flow over geologic time. A new compilation of capillary pressure and porosity (Fig. 3), measured both in reverse and normal band sets sampled in the field, clearly shows that the capillary pressure is generally higher for normal bands than for reverse bands (see supplementary material for method of capillarity calculation). This implies the presence of seals and stronger permeability anisotropy in porous sandstone reservoirs affected by tectonic extension than contraction. Such basic new rules of tectonic control of fluid flow and compartmentalization in sandstone reservoir is of major importance for both economic fluid exploration/production and CO_2 storage planning.

ACKNOWLEDGMENTS

This work was funded by a 2010–2014 project between Areva and the Laboratory Géosciences Montpellier and Grant from Ecole Doctorale Sibaghe (University of Montpellier). We thank Pr. Chia-Yu Lu from the National Taiwan University for his help in the field, associate editor James Spotila, Stephen Laubach and two anonymous reviewers for their constructive comments.

REFERENCES CITED

Antonellini, M.A., Aydin, A., and Orr, L., 1999, Outcrop-aided characterization of a faulted hydrocarbon reservoir: Arroyo Grande oil field, California, USA, *in* Haneberg, W.C., Mozley, P.S., Moore, J.C., and Goodwin, L.B., eds., Faults and Subsurface Fluid Flow in the Shallow Crust: Washington, D.C., American Geophysical Union Geophysical Monograph 113, p. 7–26, doi:10.1029/GM113p0007.

Aydin, A., 1978, Small faults formed as deformation bands in sandstone: Pure and Applied Geophysics, v. 116, p. 913–930, doi:10.1007/BF00876546.

Ballas, G., Soliva, R., Benedicto, A., and Sizun, J.-P., 2014, Control of tectonic setting and large-scale faults on the basin-scale distribution of deformation bands in porous sandstone (Provence, France): Marine and Petroleum Geology, v. 55, p. 142–159, doi:10.1016/j.marpetgeo.2013.12.020.

Ballas, G., Fossen, H., and Soliva, R., 2015, Factors controlling permeability of cataclastic deformation bands and faults in porous sandstone reservoirs: Journal of Structural Geology, v. 76, p. 1–21, doi:10.1016/j.jsg.2015.03.013.

Davatzes, N.C., and Aydin, A., 2003, Overprinting faulting mechanisms in high porosity sandstones of SE Utah: Journal of Structural Geology, v. 25, p. 1795–1813, doi:10.1016/S0191-8141(03)00043-9.

Eichhubl, P., Hooker, J., and Laubach, S.E., 2010, Pure and shear-enhanced compaction bands in Aztec Sandstone: Journal of Structural Geology, v. 32, p. 1873–1886, doi:10.1016/j.jsg.2010.02.004.

Fortin, J., Shubnel, A., and Guégen, Y., 2005, Elastic wave velocities and permeability evolution during compaction of Bleurswiller Sandstone: International Journal of

Rock Mechanics and Mining Sciences, v. 42, p. 873–889, doi:10.1016/j.ijrmms.2005.05.002.

Fossen, H., and Bale, A., 2007, Deformation bands and their influence on fluid flow: The American Association of Petroleum Geologists Bulletin, v. 91, p. 1685–1700, doi:10.1306/07300706146.

Fossen, H., R.A. Schultz, Z.K. Shipton, and K. Mair, 2007, Deformation bands in sandstone: a review: Journal of Geological Society, London, v. 164, p. 755–769, doi: 10.1144/0016-76492006-036.

Fossen, H., Zuluaga, L.F., Ballas, G., Soliva, R., and Rotevatn, A., 2015, Contractional deformation of porous sandstone: Insights from the Aztec Sandstone in the footwall to the Sevier-age Muddy Mountains thrust, SE Nevada, USA: Journal of Structural Geology, v. 74, p. 172–184, doi:10.1016/j.jsg.2015.02.014.

Klimczak, C., and Schultz, R.A., 2013, Fault damage zone origin of the Teufelsmauer, Subhercynian Cretaceous Basin, Germany: International Journal of Earth Sciences, v. 102, p. 121–138, doi:10.1007/s00531-012-0794-z.

Nicol, A., Childs, C., Walsh, J.J., and Schafer, K.W., 2013, A geometric model for the formation of deformation band clusters: Journal of Structural Geology, v. 55, p. 21–33, doi:10.1016/j.jsg.2013.07.004.

Saillet, E., and Wibberley, C.A.J., 2010, Evolution of cataclastic faulting in high-porosity sandstone, Bassin du Sud-Est, Provence, France: Journal of Structural Geology, v. 32, p. 1590–1608, doi:10.1016/j.jsg.2010.02.007.

Schultz, R.A., and Balasko, C.M., 2003, Growth of deformation bands into echelon and ladder geometries: Geophysical Research Letters, v. 30, p. 2033–2036, doi:10.1029/2003GL018449.

Schultz, R.A., and Fossen, H., 2002, Displacement-length scaling in three dimensions: The importance of aspect ratio and application to deformation bands: Journal of Structural Geology, v. 24, p. 1389–1411, doi:10.1016/S0191-8141(01)00146-8.

Schultz, R.A., Soliva, R., Fossen, H., Okubo, C., and Reeves, D.M., 2008, Dependence of displacement-length scaling relations for fractures and deformation bands on the volumetric changes across them: Journal of Structural Geology, v. 30, p. 1405–1411, doi:10.1016/j.jsg.2008.08.001.

Soliva, R., Schultz, R.A., Ballas, G., Taboada, A., Wibberley, C.A.J., Saillet, E., and Benedicto, A., 2013, A model of strain localization in porous sandstone as a function of tectonic setting, burial and material properties; new insight from Provence (SE France): Journal of Structural Geology, v. 49, p. 50–63, doi:10.1016/j.jsg.2012.11.011.

Solum, J.G., Brandenburg, J.P., Naruk, S.J., Kostenko, O.V., Wilkins, S.J., and Schultz, R.A., 2010, Characterization of deformation bands associated with normal and reverse stress states in the Navajo Sandstone, Utah: The American Association of Petroleum Geologists Bulletin, v. 94, p. 1453–1475, doi:10.1306/01051009137.

Wibberley, C.A.J., Petit, J.-P., and Rives, T., 2007, The mechanics of fault distribution and localization in high-porosity sands, Provence, France, *in* Lewis, H., and Couples, G.D., eds., The relationship between damage and localization: Geological Society, London, Special Publications 289, p. 19–46, doi:10.1144/SP289.3.

Wong, T.-f., and Baud, P., 2012, The brittle-ductile transition in porous rock: A review: Journal of Structural Geology, v. 44, p. 25–53, doi:10.1016/j.jsg.2012.07.010.

FIGURE CAPTIONS

Figure 1. Examples of geometry and spatial distribution of band sets formed as reverse and normal Andersonian regimes. (A) Reverse set of SECBs in Valley of Fire Sate Park (Nevada, USA) seen as limiting red oxidations. (B) Reverse set of CSBs in the Les Crans quarry (Provence, France). (C) Normal SB cluster adjacent to normal fault surface near Goblin Valley State Park (Utah, USA). (D) Normal SB cluster at the vicinity of two fault surfaces in the Boncavaï quarry (Provence, France). (E) Histograms of number of band per meter versus distance along scan lines for various reverse band sets. (F) Same type of histograms as shown in E, for normal band sets. Zones striped in gray mark intervals where the sandstone is not exposed.

Figure 2. Data set synthesis of reverse (black dots), normal (open dots) and strike-slip (grey dots) band sets plotted as *cluster factor* versus *maximum value of bands per meter*. Schemes of synthetic data distribution are shown for different values of Cluster Factor. Band sets are numbered, and references and number of bands per set can be found in supplementary material.

Figure 3. Compiled data of capillary pressure and porosity measured on samples from reverse and normal bands. Squares and dots are for direct and indirect measures, respectively, see supplementary material for method and data references.

[1]GSA Data Repository item 2015xxx, xxxxxxxx, is available online at www.geosociety.org/pubs/ft2015.htm, or on request from editing@geosociety.org or Documents Secretary, GSA, P.O. Box 9140, Boulder, CO 80301, USA.

Figure 1

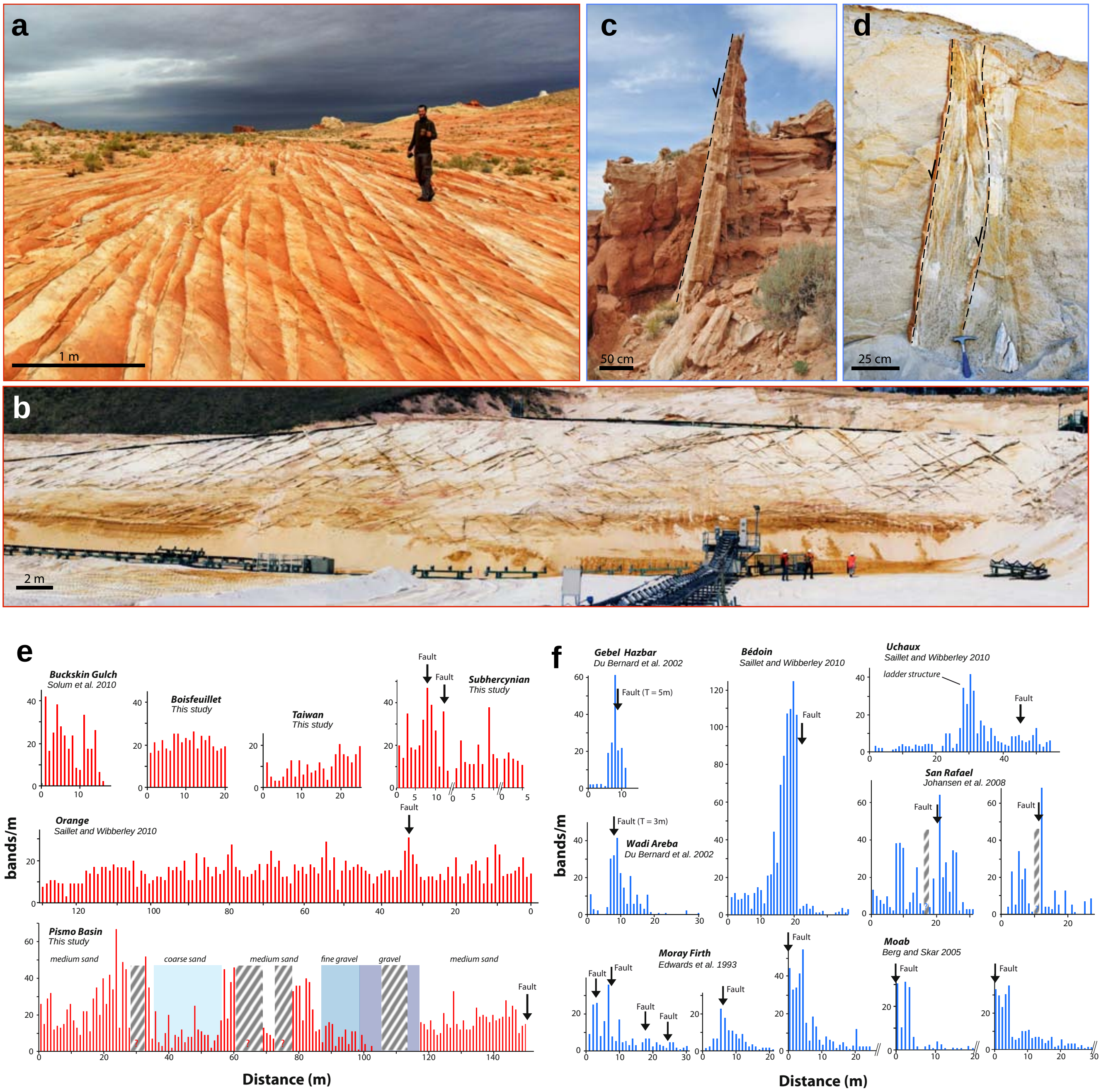
a
1 m
c
50 cm
d
25 cm
b
2 m
e
Buckskin Gulch
Solum et al. 2010
Boisfeuillet
This study
Taiwan
This study
Subhercynian
This study
Fault
Orange
Saillet and Wibberley 2010
Pismo Basin
This study
medium sand
coarse sand
medium sand
fine gravel
gravel
medium sand
bands/m
Distance (m)
f
Gebel Hazbar
Du Bernard et al. 2002
Fault (T = 5m)
Fault (T = 3m)
Wadi Areba
Du Bernard et al. 2002
Bédoin
Saillet and Wibberley 2010
Uchaux
Saillet and Wibberley 2010
ladder structure
San Rafael
Johansen et al. 2008
Moray Firth
Edwards et al. 1993
Moab
Berg and Skar 2005
Fault
bands/m
Distance (m)

Figure 2

Figure 2

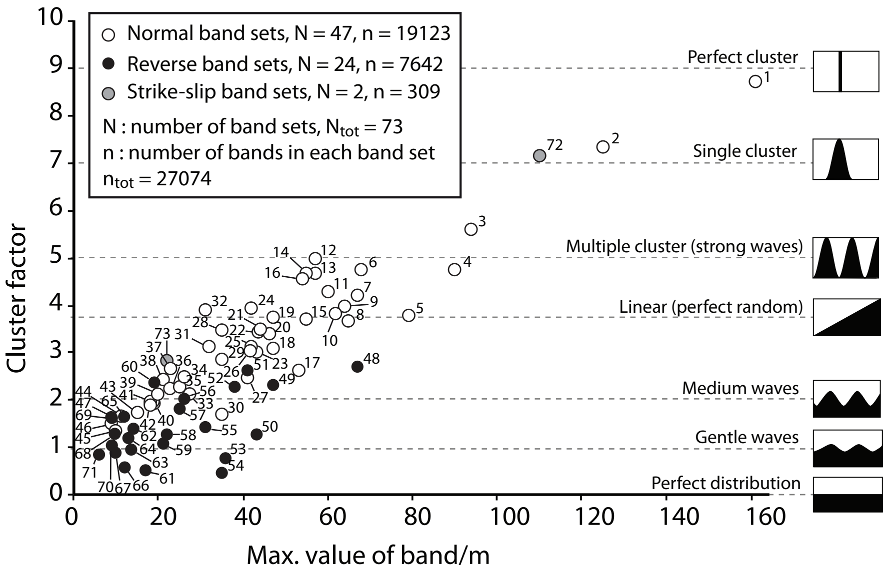

Figure 3

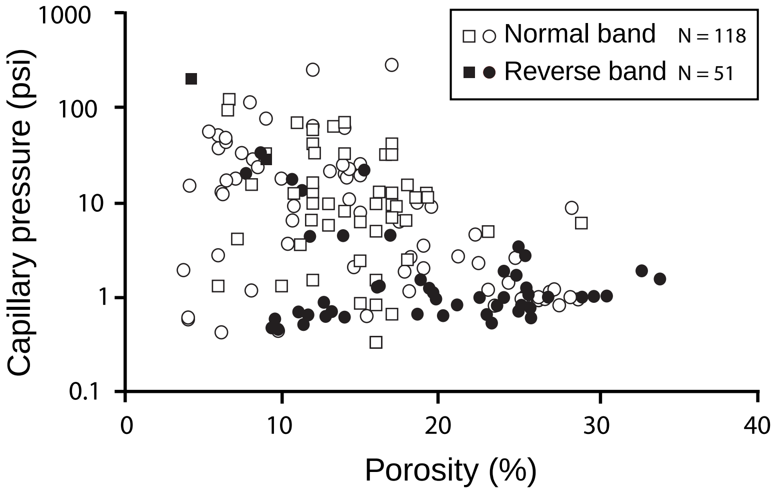

Normal band N = 118
Reverse band N = 51
Capillary pressure (psi)
1000
100
10
1
0.1
0
10
20
30
40
Porosity (%)

Supplementary material 1: References for data in figure 2

1.1 Normal band sets

1 : Delicate Arch (Antonellini and Aydin, 1995), n = 1710
2 : Bédoin 3 (Saillet and Wibberley, 2010), n = 875
3 : Moab 3 (Davatzes and Aydin, 2003), n = 855
4 : Moab 2 (Davatzes and Aydin, 2003), n = 1707
5 : Gebel Samra (Du Bernard et al., 2002), n = 951
6 : San Rafael 1 (Johansen and Fossen, 2008), n = 244
7 : Moab 1 (Fossen et al., 2005), n = 858
8 : Slickrock (Fossen et al., 2005), n = 381
9 : San Rafael 2 (Johansen and Fossen, 2008), n = 441
10 : San Rafael 4 (Johansen and Fossen, 2008), n = 371
11 : Gebel Hazbar (Du Bernard et al., 2002), n = 166
12 : Arches Navajo (Antonellini and Aydin, 1994), n = 428
13 : San Rafael 5 (Johansen and Fossen, 2008), n = 127
14 : Moab 8 (Berg and Skar, 2005), n = 321
15 : San Rafael 3 (Johansen and Fossen, 2008), n = 459
16 : Arches Morisson (Antonellini and Aydin, 1994), n = 172
17 : Wadi Taiba 2 (Beach et al. 1999), n = 244
18 : Hidden Canyon 6 (Johansen and Fossen, 2008), n = 690
19 : Wadi Taiba 1 (Beach et al. 1999), n = 1159
20 : Hidden Canyon 2 (Johansen and Fossen, 2008), n = 285
21 : Hidden Canyon 1 (Johansen and Fossen, 2008), n = 404
22 : Moab Entrada (Antonellini and Aydin, 1994), n = 151
23 : Bédoin 1 (Saillet and Wibberley, 2010), n = 631
24 : Wadi Areba (Du Bernard et al., 2002), n = 227
25 : Uchaux S1 (Saillet and Wibberley, 2010), n = 403
26 : Naqb Budra (Du Bernard et al., 2002), n = 362
27 : Bédoin 2 (Saillet and Wibberley, 2010), n = 388
28 : Moab 7 (Berg and Skar, 2005), n = 283
29 : Moray Firth 2 (Edwards et al., 1993), n = 230
30 : Gebel Heckma (Du Bernard et al., 2002), n = 365
31 : Moab 4 (Davatzes and Aydin, 2003), n = 230
32 : Moab 5 (Berg and Skar, 2005), n = 154
33 : Moab Morisson (Antonellini and Aydin, 1994), n = 261
34 : Egypt (Schueller et al., 2013), n = 110
35 : Uchaux N2 (Saillet and Wibberley, 2010), n = 146
36 : Moray Firth 4 (Edwards et al., 1993), n = 130
37 : Golf course (Farrel et al., 2014), n = 89
38 : Moray Firth 3 (Edwards et al., 1993), n = 70
39 : Moab 6 (Berg and Skar, 2005), n = 195
40 : Uchaux S2 (Saillet and Wibberley, 2010), n = 258
41 : Clashach (Farrel et al., 2014), n = 854
42 : Valley of Eden (Fowles and Burley, 1994), n = 110
43 : Moray Firth 1 (Edwards et al., 1993), n = 101
44 : Hidden Canyon 4 (Johansen and Fossen, 2008), n = 197
45 : Uchaux N1 (Saillet and Wibberley, 2010), n = 165

46 : Hidden Canyon 5 (Johansen and Fossen, 2008), n = 107
47 : Hidden Canyon 3 (Johansen and Fossen, 2008), n = 58

1.2 Reverse band sets

48 : Pismo Medium Grain (this study), n = 1248
49 : Subhercynian 1 (this study), n = 325
50 : Montmout (this study), n = 136
51 : Buckskin Gulch (Solum et al., 2010), n = 323
52 : Subhercynian 3 (this study), n = 68
53 : Boncavaï (this study), n = 90
54 : Sablex (this study), n = 129
55 : Orange (Saillet and wibberley, 2010), n = 3591
56 : Boisfeuillet (this study), n = 142
57 : Pismo Coarse Sand (this study), n = 310
58 : Subhercynian 2 (this study), n = 96
59 : Taiwan 2 (this study), n = 152
60 : Les Crans 2 (this study), n = 171
61 : Subhercynian 4 (this study), n = 69
62 : Bollène (this study), n = 59
63 : Bagnols (this study), n = 62
64 : Taiwan 1 (this study), n = 121
65 : Les Crans 1 (this study), n = 141
66 : Mornas (this study), n = 63
67 : Valley of Fire 1 (this study), n = 35
68 : Roquemaure (this study), n = 99
69 : Pismo Gravels (this study), n = 16
70 : Valley of Fire 2 (this study), n = 41
71 : Muddy Mountains (this study), n = 40

1.3 Strike-slip band system

72 : Bédoin 4 (this study), n = 233
73 : St Michel (this study), n = 76

1.4 References :

Antonellini, M., Aydin, A., 1994. Effect of faulting on fluid flow in porous sandstones: petrophysical properties, American Association of Petroleum Geologists Bulletin, no. 78, p. 355–377.

Antonellini, M.A., Aydin, A., 1995. Effect of faulting on fluid flow in sandstones, geometry and spatial distribution: American Association of Petroleum Geologists Bulletin, no. 78, p. 642–671.

Beach, A., Welbon, A. I., Brockbank, P. J., McCallum, J. E., 1999, Reservoir damage around faults: Outcrop examples from the Suez Rift: Petroleum Geosciences, v. 5, p. 109–116.

Berg, S. S., and T. Skar, 2005, Controls on damage zone asymmetry of a normal fault zone: Outcrop analysis of a segment of the Moab fault, SE Utah, Journal of Structural Geology, no. 27, p. 1803–1822.

DuBernard, X., Labaume, P., Darcel, C., Davy, P., Bour, O., 2002. Cataclastic slip band distribution in normal fault damage zones, Nubian sandstones, Suez rift, Journal of Geophysical Research, no. 107-B7, p. 2141–2153.

Davatzes, N.C., and Aydin A., 2003. Overprinting faulting mechanisms in high porosity sandstones of SE Utah: Journal of Structural Geology, no. 25, p. 1795–1813.

Edwards, E. H., Becker, A. D., Howell, J. A., 1993. Compartimentalization of an eolian sandstone by structural heterogeneities: Permo- Triassic Hopeman Sandstone, Moray Firth, Scotland, *in* Characterization of Fluvial and Aeolian Reservoirs, eds., C. P. North and D. J. Prosser, Geological Society [London], Special Publications 73, p. 339– 365.

Farell, N.J.C., Healy, D., Taylor, C.W., 2014. Anisotropy of permeability in faulted porous sandstones, Journal of Structural Geology, No. 63, p. 50–67.

Fossen, H., Johansen, T.E.S., Hesthammer, J., Rotevatn, A., 2005. Fault interaction in porous sandstone and implications for reservoir management; examples from southern Utah, American Association of Petroleum Geologists Bulletin, no. 89, p. 1593–1606.

Fowles, J., Burley, S., 1994. Textural and permeability characteristics of faulted, high porosity sandstones, Marine and Petroleum Geology, no. 11, p. 608–623.

Johansen, T.E.S., Fossen, H., 2008. Internal geometry of fault damage zones in interbedded siliciclastic sediments, *in* Wibberley, C.A.J., Kurz, W., Imber, J., Holdsworth, R.E. Collettini, C., eds., The internal structure of fault zones: Implications for mechanical and fluid-flow properties, Geological Society [London], Special Publications 299, p. 35–56.

Johansen, T.E.S., Fossen, H., 2008. Internal geometry of fault damage zones in interbedded siliciclastic sediments, *in* Wibberley, C.A.J., Kurz, W., Imber, J., Holdsworth, R.E. Collettini, C., eds., The internal structure of fault zones: Implications for mechanical and fluid-flow properties, Geological Society [London], Special Publications 299, p. 35–56.

Saillet, E., Wibberley, C.A.J., 2010. Evolution of cataclastic faulting in high-porosity sandstone, Bassin du Sud-Est, Provence, France: Journal of Structural Geology, no. 32, p. 1590–1608.

Schueller, S., Braathen, A., Fossen, H., Tveranger, J., 2013. Spatial distribution of deformation bands in damage zones of extensional faults in porous sandstones: statistical analysis of field data, Journal of Structural Geology, no. 52, p. 148–162.

Supplementary material 2: Mechanical explanation

2.1 Porous sandstone mechanical behaviour and stress paths for contraction and extension

Mechanical tests in porous sandstones generally show a localized Byerlee-type shear behavior at low to moderate applied mean stresses (relative to P^*, the maximum means stress supported by the material), and a more distributed compactional/cataclastic behavior at relatively high mean stresses (yield Cap envelope, e.g. Wong and Baud, 2012; Rutter and Glover, 2013) (see Figure 1 in supplementary material). In geologic conditions, for a given initial lithostatic stress state (burial stress path), tectonic contraction increases first the mean stress in the rock, and later the differential stress. This contractional stress path makes the material more probable to yield in a compactional behavior along the Cap envelope (see the red stress path in Figure 1). In contrast, tectonic extension reduces the mean stress with a synchronous differential stress increase, leading the material to fail in a more frictional-shearing Byerlee-type behaviour (see the blue stress path). Details for the calculation of these stress paths are exposed in Soliva et al., 2013.

These expected strong differences both in mechanical behavior and stress path give the basic premises to explain the different types of clustering observed between reverse and normal regimes. Mechanical tests generally show brittle fractures or cataclastic SBs formed in Byerlee condition (e.g. Fortin et al, 2005), which generally allow shear localization and stress relaxation limiting significant band creation outside the shear zone (Schultz and Soliva, 2012). In contrast, cataclastic “compactional” bands (comparable to CSBs, SECBs and PCB observed in the field) form along the yield cap envelope with little or no stress relaxation, keeping the sandstone critically stressed in its volume. This allows subsequent compactional band development and infill into the whole sample. Important differences however rise between mechanical test and nature such as large thickness of SBs clusters observed in the field compared to SBs formed in test. This probably finds explanation in the difference of sample scale and boundary conditions between mechanical test and nature.”

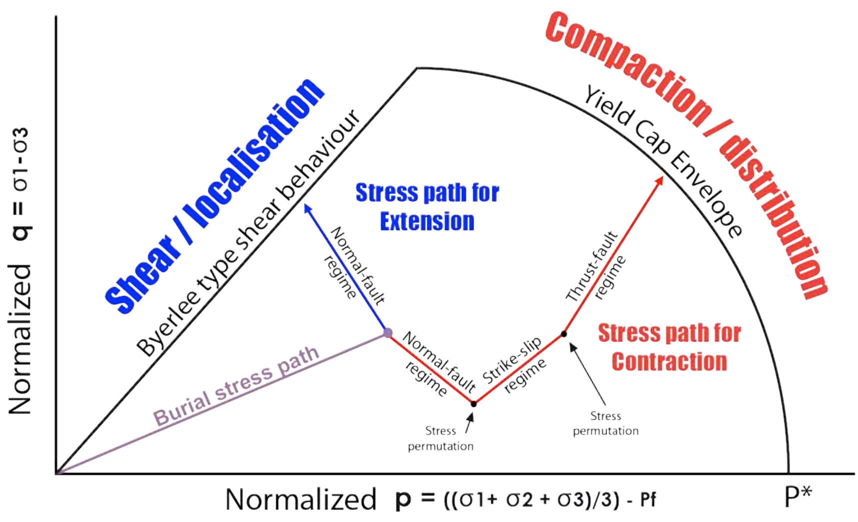

Figure 1. Graph of normalized differential stress (q) and mean stress (p) showing the yield strength envelope for porous sandstones and the burial and tectonic stress path for contraction and extension. Stress path for extension favours shear strain localisation due to a Byerlee type mechanical behaviour, whereas stress path for contraction allows compactional strain distribution due to a yield cap compactional behaviour.

2.2 References

Fortin, J., Shubnel, A., Guégen, Y., 2005. Elastic wave velocities and permeability evolution during compaction of Bleurswiller Sandstone. Int. J. Rock Mech. Min. Sci., 42, 873–889.

Rutter, E.H., Glover, C.T., 2012. The deformation of porous sandstones; are Byerlee friction and the critical state line equivalent? Journal of Structural Geology, no. 44, p. 129–140.

Schultz, R.A, Soliva, R., 2012. Propagation energies inferred from deformation bands in sandstone. International Journal of Fracture, no. 176, p. 135-149, doi:10.1007/s10704-012-9730-2.

Wong, T-f., Baud, P., 2012. The brittle-ductile transition in porous rock: A review: Journal of Structural Geology, no. 44, p. 25–53.

Supplementary material 3: Capillary Pressure Method

The capacity for a fluid to pass through a porous media depends on the pressure applied to this fluid. A minimum pressure, called capillary pressure (*Pc*), is necessary for a non-wetting fluid (hydrocarbon, mercury) to displace a wetting fluid (air, water) in a porous network composed of pores and connections (Pittman 1992). In the figure 3, we synthesized direct measures of capillary pressure in apparatus from the following papers: Gibson (1998), Ogilvie and Glover (2001), Tueckmantle et al. (2010), and Torabi et al. (2013). We completed this data set with indirect measures of capillary pressures calculated from porosity, permeability, or pore access radius data described in the following references: Fowles and Burley (1994), Lothe et al. (2002), Al-Hinaï et al. (2008), Aydin and Ahmadov (2009), Sun et al. (2011), Ballas et al. (2013) and Ballas et al. (2014). Methods used for capillary pressure calculation are exposed below (see Torabi et al., 2013 for detailed explanation). Data are classified between structures coming from extensional tectonic regime and contractional tectonic regime. These data are used to reveal the ability of a fault to act as a barrier or conduit to fluid flow (Torabi et al., 2013).

2.1 Capillary pressure calculated from Mercury Injection-Capillary Pressure (MICP)

The capillary pressure can be estimated using a graphical method from MICP data (Katz and Thompson, 1986). Because this point is generally difficult to obtain, the Washburn's equation (1921) is generally used to estimate the capillary pressure form MICP data:

$$Pc = \frac{2\gamma \cos \Phi}{R} \qquad (1)$$

With: *Pc* = Capillary Pressure (psi)

γ = Two-phase fluid interfacial tension (480 dynes/cm for Mercury/Air)

Φ = Contact angle between two-phase fluids and solid (140° for Mercury/Air)

R = Effective pore-access radius (μm), corresponding to the apex point on a graph showing Hg saturation/pressure vs Hg saturation (Pittman 1992).

The *Pc* obtained with the equation (1) is converted for a two-phase fluids oil/water using the following equation:

$$Pc\ (oil/water) = \frac{31}{485}\, Pc\ (\mathrm{Hg}/air) \qquad (2)$$

2.2 Capillary pressure from Porosity-Permeability data

Empirical relationship (3) between porosity, permeability and effective pore-access radius was established from 800 sandstone samples by Pittman (1992).

$$Log\ (R) = -0.117 + 0.475 \log (k) - 0.099 \log (n) \qquad (3)$$

With: *R* = Effective pore-access radius (μm)

k = Permeability (mD)

n = Porosity

This effective pore-access radius is used in the equation (1) to calculate the capillary pressure.

2.3 References

Al-Hinai, S., Fisher, Q.J., Al-Busafi, B., Guise, P., Grattoni, C.A., 2008. Laboratory measurements of the relative permeability of cataclastic fault rocks: an important consideration for production simulation modelling. Marine and Petroleum Geology 25, 473–485.

Aydin, A., Ahmadov, R., 2009. Bed-parallel compaction bands in aeolian sandstone: Their identification, characterization and implications. Tectonophysics 479, 277-284.

Ballas, G., Soliva, R., Sizun, J-P., Fossen, H., Benedicto, A., Skurtveit, E., 2013. Shear-enhanced compaction bands formed at shallow burial conditions; implications for fluid flow (Provence, FRANCE). Journal of Structural Geology 47, 3–15.

Ballas, G., Soliva, R., Benedicto, A., Sizun, J-P., 2014. Control of tectonic setting and large-scale faults on the basin-scale distribution of deformation bands in porous sandstone (Provence, France). Marine and Petroleum Geology 55, 142–159.

Fowles, J., Burley, S., 1994. Textural and permeability characteristics of faulted, high porosity sandstones. Marine and Petroleum Geology 11, 608–623.

Gibson, R.G., 1998. Physical character and fluid-flow properties of sandstone-derived fault zones. In: Coward, M.P., Daltaban, T.S., Johnson, H., (Eds.), Structural Geology in Reservoir Characterization. Geological Society, London, Special Publications 127, 83–97.

Katz, A.J., Thompson, A.H., 1986. Quantitative prediction of permeability in porous rock. Physical Review B34, 8179–8181.

Lothe, A.E., Gabrielsen, R.H., Bjørnevoll Hagen, N., Larsen, B.T., 2002. An experimental study of the texture of deformation bands : effects on porosity and permeability of sandstones. Petroleum Geoscience 8, 195–207.

Ogilvie, S.R., Glover, P.W.J., 2001. The petrophysical properties of deformation bands in relation to their microstructure. Earth and Planetary Science Letters 193, 129–142.

Pittman, E.D., 1992. Relationship of Porosity and Permeability to Various Parameters Derived from Mercury Injection-Capillary Pressure Curves for Sandstone. American Association of Petroleum Geologists Bulletin 76, 191–198.

Sun, W., Andrade, J.E., Rudnicki, J.W., Eichhubl, P., 2011. Connecting microstructural attributes and permeability from 3D tomographic images of in situ shear-enhanced compaction bands using multiscale computations. Geophysical Research Letters 38, L10302.

Torabi, A., Fosse, H., Braathen, A., 2013. Insight into petrophysical properties of deformed sandstone reservoirs. American Association of Petroleum Geologists Bulletin 97, 619–637.

Tueckmantel, C., Fisher, Q.J., Knipe, R.J., Lickorish, H., Khalil, S.M., 2010. Fault seal prediction of seismic-scale normal faults in porous sandstone: A case study from the eastern Gulf of Suez rift, Egypt. Marine and Petroleum Geology 27, 334–350.

Washburn, E.W., 1921. Note on a method of determining the distribution of pore sizes in a porous material. Proceeding of the National Academy of Science 7, 115–116.